A NASTRAN DMAP ALTER FOR LINEAR BUCKLING **N89-22948**

ANALYSIS UNDER DYNAMIC LOADING

Robert A. Aiello and Joseph E. Grady
National Aeronautics and Space Administration
Lewis Research Center
Cleveland, Ohio 44135

SUMMARY

A unique modification to the NASTRAN solution sequence for transient analysis with direct time integration (COSMIC NASTRAN rigid format 9) has been developed and incorporated into a DMAP alter. This DMAP alter calculates the buckling stability of a dynamically loaded structure, and is used to predict the onset of structural buckling under stress-wave loading conditions. The modified solution sequence incorporates the linear buckling analysis capability (rigid format 5) of NASTRAN into the existing Transient solution rigid format in such a way as to provide a time dependent eigensolution which is used to assess the buckling stability of the structure as it responds to the impulsive load. As a demonstration of the validity of this modified solution procedure, the dynamic buckling of a prismatic bar subjected to an impulsive longitudinal compression is analyzed and compared to the known theoretical solution. In addition, a dynamic buckling analysis is performed for the analytically less tractable problem of the localized dynamic buckling of an initially flawed composite laminate under transverse impact loading. The addition of this DMAP alter to the transient solution sequence in NASTRAN facilitates the computational prediction of both the time at which the onset of dynamic buckling occurs in an impulsively loaded structure, and the dynamic buckling mode shapes of that structure.

INTRODUCTION

Composite laminates that are subjected to static, dynamic, or fatigue loading are known to undergo delamination, or debonding, between the laminated plies of which they are composed. Delamination causes a significant loss stiffness and strength, and can considerably reduce the structural integrity of a laminate. Once this damage has occurred, a compressive stress near the delamination can induce local buckling of the delaminated plies. This buckling may then cause further extension of the delamination and progressive weakening of the laminate. In lieu of actual experimental testing, the ability to computationally predict the onset of delamination buckling is necessary for evaluating the durability of many composite structures.

The delamination buckling phenomenon has been observed experimentally under both static and fatigue loading conditions (Refs. 1 to 4), and several analytical and numerical methods have been proposed (Refs. 5 and 6) to model this damage mechanism. Finite-element approaches (Refs. 7 to 9) have been used as the basis for these analyses, but no comparable numerical methods exist to analyze delimination buckling which occurs as a result of an impulsively applied load. That is the topic of this paper.

Experimental observations of dynamic delamination buckling in transversely impacted laminates were reported earlier (Refs. 10 to 12), using high-speed photography and simultaneous strain measurements of transversely impacted laminates. A related numerical analysis (Ref. 10) indicated that the buckling behavior must be accounted for in the computational model in order to accurately assess the damage tolerance capability of the laminate. This motivated the present development of a NASTRAN DMAP alter analysis procedure that can be used to computationally predict the onset of buckling instability under transient stress-wave loading.

The objectives of this paper are, therefore, (1) to outline the dynamic buckling analysis computational procedure and its implementation into the DMAP alter sequence (2) demonstrate the validity of the dynamic buckling analysis procedure by analyzing a simple one-dimensional example problem with a known solution, and (3) apply the dynamic buckling analysis to the analytically less tractable problem of the localized dynamic buckling of an initially flawed composite laminate under transverse impact loading.

The NASTRAN transient solution sequence, when modified as indicated in the following section, provides a new computational tool that can be used to predict both the time at which the onset of dynamic buckling occurs and the dynamic buckling mode shapes of an impulsively loaded structure.

Dynamic Buckling Analysis

Linear buckling analysis requires solution of the eigenvalues problem:

$$\left[[K] + \lambda [K_\sigma] \{\phi\} = 0 \right]$$ (1)

where

[K]   structural stiffness matrix;

$[K_\sigma]$ stress stiffness matrix

λ, $\{\phi\}$ denote the associated eigenvalue and eigenvector

In terms of the buckling analysis, the eigenvector $\{\phi\}$ represents the buckling mode shape, and the associated eigenvalue λ indicates the multiple of $[K_\sigma]$ needed to make equation (1) singular, that is, to cause buckling. In a one-dimensional column buckling problem, each scalar eigenvalue satisfying equation (1) physically represents the nondimensional ratio:

$$\lambda = \frac{\sigma A}{P_*}$$ (2)

where σ is the compressive stress in the column, A is the cross-sectional area, and P_* is the buckling load. If the eigenvalue has the critical value of unity ($\sigma A = P_*$), buckling in the associated mode occurs.

In the dynamic case, the terms of $[K_\sigma]$ in Eq. (1) vary with time as the stress waves propagate through the structure. The eigensolution of (1) then

becomes time dependent, and can be used to track the buckling stability as a function of time. Figure 1 is a simplified representation of a modified direct-time integration solution sequence in which the updated stress stiffness matrix is formed after each time step Δt, and the associated eigenvalue problem in equation (1) is solved. The eigenvalue is now a function of time, and it indicates the onset of buckling when it reaches the critical value of unity. Figure 2 is the DMAP alter which incorporates this dynamic buckling algorithm into the existing transient solution sequence.

DMAP Procedure

The functions of the DMAP statements shown in Fig. 2 are summarized here. In line 2 the number of columns in the UPV matrix is determined. This matrix contains the displacement, velocity and acceleration vectors for each degree of freedom at each time step. Lines 2 through 16 follow the Bubble Algorithm approach of Ref. 13. The DMI column matrices TIP1 and BAS1 from the Bulk Data deck, each initially sized to contain more rows than columns in the UPV matrix, are used to form two new column matrixes, MNTRJ and BOOTI. The number of rows in each of these matrices is equal to the number of columns in the UPV matrix. The monitor matrix MNTRJ initially contains unity in the first row and zero in the remaining rows. The BOOTI matrix always contains unity in the last row and zero in the remaining rows.

Having determined the size of the partitioning matrices, the eigenvalue extraction data is determined in line 19 and the buckling calculations are now performed. At the beginning of each pass through the RAALOOP, corresponding to each integration time step of the requested output, the current column position is compared with the number of columns in the UPV matrix, lines 25 through 27, ending the loop at the end of the available data. Continuing within the loop the unity value of the MNTRJ matrix is advanced three rows, lines 28 through 31, pointing to the location of the current displacement vector in the UPV matrix. The MNTRJ matrix is used to partition the UPV matrix, line 32, stripping the column containing the displacements. These displacements are used in the DSMG1 module, line 33, to form the time-varying global differential stiffness matrix, KDGG. The reduced differential stiffness matrix, KDAA, is then formed by eliminating the restrained and dependent degrees of freedom, line 35 through 45, and in line 47 this matrix is multiplied by negative one, forming the KDAAM matrix. The stiffness matrices KAA and KDAAM are then used in the READ module, line 48, to solve for the eigenvalues and eigenvectors for each integration time step initially requested for output.

The eigenvalue for each time step is printed by line 52. Optionally, lines 53 and 54 may be used to print eigenvalues and eigenvalue extraction data. Line 58 may be used to print eigenvectors. The RAALOOP is ended at line 64.

The computationally intensive nature of this analysis can be made more efficient by slightly modifying the DAMP procedure. A promising method is to perform the buckling analysis at specified time intervals in the transient solution sequence rather than after every time step, as is done here. The length of the time interval can be progressively decreased as the eigenvalue begins to change more rapidly, or as the critical value of unity is approached.

This technique will significantly reduce the number of individual buckling analyses performed, and hence will result in a more computationally efficient algorithm.

Example Problem

In order to establish the validity of this analysis procedure, a simple problem with a known solution, as given in Ref. 14, was analyzed. The propagation of a longitudinal compressive pulse in a long prismatic bar, shown in Fig. 3, was modelled.

Assuming a one-inch diameter aluminum bar of uniform circular cross section the elastic and geometric constants are:

$$E = 10 \times 10^6 \text{ psi} \tag{3}$$

$$I = \frac{\pi r^4}{4} = \frac{\pi}{64} \text{ in.}^4 \tag{4}$$

$$A = \pi r^2 = \frac{\pi}{4} \text{ in.}^2 \tag{5}$$

$$\rho = 2.5 \times 10^{-4} \frac{\text{lb} \cdot \text{s}^2}{\text{in.}^4} \tag{6}$$

$$L = 100 \text{ in.} \tag{6}$$

where E is the Young's Modulus, I is the area moment of inertia, A is the cross-sectional area, ρ is the mass density, and L is the length of the bar.

The lowest buckling load is given by (Ref. 15):

$$P_* = \frac{\pi^2 EI}{4L^2} = 121 \text{ lb} \tag{7}$$

As shown in Fig. 3, the applied load is identical to the static buckling load in Eq. (7).

Using the above material constants, the bar wave velocity is given by (Ref. 14):

$$C_0 = \sqrt{\frac{E}{\rho}} = 200,000 \frac{\text{in.}}{\text{sec}} \tag{8}$$

so the time for the longitudinal compression wave to travel from the impact point to the distal end of the bar is

$$t_0 = \frac{L}{C_0} = 500 \text{ μs} \tag{9}$$

190

A NASTRAN model consisting of ten rod elements, for a total of ten unconstrained axial degrees of freedom, was used to model the longitudinal impact of the bar. The integration time step was taken as

$$\Delta t = \frac{1}{4} \frac{L}{10C_O} = 12.5 \ \mu s \tag{10}$$

to insure a numerically converged solution. The propagation of the compression wave from the point of impact to the clamped end of the bar is depicted in Figs. 4(a) and (b).

The compressive pulse, traveling at a speed C_O, reaches the complete length of the bar at time t_O (500 μs). Because the distal end of the bar is held fixed, the incident compressive pulse reflects (Ref. 15) as a pulse of the same sign (compressive) which superimposes on the existing uniform compressive stress in the bar. Figures 4(c) and (d) depict the progression of the reflected pulse, traveling at a speed C_O, back to the proximal end of bar, effectively doubling the compressive load supported by the bar. Reflecting from the proximal (free) end as a pulse of opposite sign (tensile) which superimposes on the existing compressive stress, the bar returns to its original fully stressed state at time $3t_O$, (1500 μs) as shown in Figs. 4(e) and (f). Finally, in Figs. 4(g) and (h), the tensile pulse reflects as a tensile pulse from the fixed end which temporarily cancels the uniform compression at time $4t_O$ (2000 μs), leaving the bar instantaneously unstressed. The stress states depicted in Figs. 4(i) and (j), for all practical purposes identical to those in Figs. 4(a) and (b), indicate that, assuming no damping exists, the above cycle will repeat itself indefinitely.

The corresponding time dependence of the lowest eigenvalue is shown in Fig. 5. The critical value of 1.0 is reached at times t_O, $3t_O$, $5t_O$, $7t_O$,. . . (500, 1500, 2500, 3500 μs,. . .); and whenever the bar supports a uniform compressive stress corresponding to its buckling load. Similarly, the eigenvalue reaches to its lower limit of 0.5 at times $2t_O$, $6t_O$, $10t_O$,. . . (1000, 3000, 5000 μs,. . .); and whenever the stress state is double that of the buckling load. The eigenvalue becomes large (theoretically infinite) at time 0, $4t_O$, $8t_O$,. . . (0, 2000, 4000, 6000 μs,. . .) ; and whenever the bar is unstressed.

Superimposed on the finite element results in Fig. 4 is the theoretical 1-D solution, assuming the stress wave propagates nondisperively at a constant speed C_O and reflects from the boundaries as described above. Good agreement exists between the two solutions, even when relatively few finite elements are used to model the bar. The time behavior of the lowest eigenvalue, shown in Fig. 5, can be interpreted directly in terms of the transient stress distribution in Fig. 4. Since the applied compressive load is exactly equal to the first static buckling load in Eq. (7), and no strain-rate dependence was assumed in the finite element model, buckling is predicted whenever the bar is uniformly stressed with its critical static buckling stress, which occurs at odd multiples of t_O, as shown in Fig. 4.

In a practical application, the above analysis is valid only until the onset of buckling occurs, since no post-buckling behavior has yet been included in the finite element model. The time itegration was extended in the example problem only to physically interpret the results of the dynamic buckling analysis.

The example problem could have been solved without the use of a finite element analysis because of the simple non-dispersive nature of the longitudinal wave propagation. However, the propagation of flexural waves in beam-like structures is dispersive by nature, and as such would pose a formidable challenge without the use of some type of computational simulation. In Ref. 11, experimental measurements of delamination duckling in graphite/epoxy composite laminates were reported. The beam-like experimental specimens had simulated delaminations (ply disbonds) embedded in them during the fabrication process. They were held clamped at both ends and impacted transversely, as depicted schematically in Fig. 6. The subsequent flexure-induced local buckling of the delamination was recorded using strain gages and high speed photography. A finite element model of the initially flawed experimental specimen is used here to verify that the dynamic delamination buckling phenomenon can be predicted using computational simulation. Figure 6 shows the geometry and loading conditions for the initially flawed composite laminate subjected to a transverse impact. The finite element discretization of this laminate near the embedded flaw is shown schematically in Fig. 7. The layered structure of the composite laminate is represented by layers of shell elements. Multipoint constraints are imposed on the degrees of freedom between neighboring nodal points in the thickness direction such that simple beam bending displacements are enforced; that is, plane sections remain plane and no strain exists in the thickness direction. These constraints are removed in the delaminated region to allow the delaminated plies to separate from the main laminate when a local compression occurs in that area, as shown in Fig. 7. More complete details of the finite element modeling procedure are given in Ref. 12.

The progression of the flexural waves out from the central impact point to the boundaries of the laminate are shown in Fig. 8. As the disturbance passes through the flawed region at 100 to 150 µs after impact, the delaminated ligament separates from the laminate and begins to support a compressive longitudinal stress which increases in magnitude until it causes a local buckling of the delamination. The eigenvalue behavior and corresponding buckling mode are shown in Fig. 9. As the laminate deforms under the applied load, the eigenvalue decreases monotonically in magnitude until it reaches the critical value of unity, indicating the onset of buckling at approximately 190 µs from impact. The corresponding buckling mode shape is also depicted in the figure.

These results correspond closely with experimental observations. Both the buckling mode shape and the time at which buckling occurs are in good agreement with measurements taken from high speed photographs. A detailed comparison of finite element results and experimental measurements is given in Ref. 11.

CONCLUSIONS

A dynamic delamination buckling analysis procedure has been incorporated, in the form of a DMAP alter, into the transient analysis rigid format of NASTRAN. With this enhancement, NASTRAN can be used to calculate the time at which dynamic buckling occurs and the buckling mode shape of a structure subjected to dynamic loading. Comparison of the calculated results with a known

solution supports the validity of the analysis. Application of the dynamic buckling analysis to the more complex problem of transverse impact of beam-like laminate was demonstrated, and the results phenomenologically duplicated those reported in earlier experiments.

REFERENCES

1. Gillespie, J.W.; and Pipes, R.B.: Compressive Strength of Composite Laminates with Interlaminar Defects. Composite Structures, vol. 2, no. 1, 1984, pp. 49-69.

2. Rosenfeld, M.S.; and Gause, L.W.: Compression Fatigue Behavior of Graphite/Epoxy in the Presence of Stress Raisers. Fatigue of Fibrous Composite Materials, ASTM STP-723, K.N. Lauraitis, ed., American Society for Testing and Materials, 1981, pp. 174-196.

3. Konishi, D.Y.; and Johnston, W.R.: Fatigue Effects on Delaminations and Strength Degradation in Graphite/Epoxy Laminates. Composite Materials: Testing and Design (Fifth Conference), ASTM STP-674, S.W. Tsai, ed., American Society for Testing and Materials, 1979, pp. 597-619.

4. Chai, H.; Knauss, W.G.; and Babcock, C.D.: Observation of Damage Growth in Compressively Loaded Laminates. Exper. Mech., vol. 23, no. 3, Sept. 1983, pp. 329-337.

5. Simitses, G.J.; and Sallam, S.: Delamination Buckling and Growth of Flat Composite Structural Elements. AFOSR-85-1067TR, Sept. 1984. (Avail. NTIS, AD-A162370).

6. Kardomateas, G.A.; and Schmueser, D.W.: Buckling and Postbuckling of Delaminated Composites under Compressive Loads Including Transverse Shear Effects. AIAA J., vol. 26, no. 3, Mar. 1988, pp. 337-343.

7. Whitcomb, J.D.: Finite Element Analysis of Instability Related Delamination Growth. J. Compos. Mater., vol. 15, no. 5, Sept. 1981, pp. 403-426.

8. Kapania, R.K.; and Wolfe, D.R.: Delamination Buckling and Growth in Axially Loaded Beam-Plates. 28th Structures, Structural Dyanmics, and Materials Conference, Part 1, AIAA, 1987, pp. 766-775.

9. Whitcomb, J.D.; and Shivakumar, K.N.: Strain-Energy Release Rate Analysis of a Laminate with a Postbuckled Delamination. NASA TM-89091, 1987.

10. Sun, C.T.; and Grady, J.E.: Dyanmic Delamination Crack Propagation in a Graphite/Epoxy Laminate. Composite Materials: Fatigue and Fracture, ASTM STP-907, H.T. Hahn, ed., American Society for Testing and Materials, 1986, pp. 5-31.

11. Grady, J.E.; and De Paula, K.J.: Measurement of Impact-Induced Delamination Buckling in Composite Laminates. Dynamic Failure, Proceedings of the 1987 SEM Fall Conference, Society for Experimental Mechanics, Bethel, CT, 1987, pp. 160-168.

12. Grady, J.E.; Chamis, C.C.; and Aiello, R.A.: Dyanamic Delamination Buckling in Composite Laminates under Impact Loading: Computational Simulation. NASA TM-100192, 1987.

13. Pamidi, P.R.; and Butler, T.G.: Bubble Vector in Automatic Merging. Fifteenth NASTRAN Users' Colloquim, NASA CP-2481, 1987, pp. 118-135.

14. Graff, K.F.: Wave Motion in Elastic Solids. Ohio State University Press, 1975, pp. 75-139.

15. Timoshenko, S.P.: Strength of Materials. 2nd ed., D. Van Nostrand Company, Inc., 1941.

DYNAMIC BUCKLING ALGORITHM

```
┌──────────────────┐
│  READ INPUT DATA │
└──────────────────┘
         │
         ▼
┌──────────────────┐
│ ASSEMBLE STIFFNESS,│
│  MASS MATRICES   │
└──────────────────┘
         │
         ▼
┌──────────────────┐
│ PARTITION MATRICES│
└──────────────────┘
         │
         ▼
┌──────────────────┐
│  FORM APPLIED    │
│  LOAD VECTOR     │
└──────────────────┘
         │
         ▼
┌──────────────────┐
│ INTEGRATE EQUATIONS│
│ OF MOTION:        │
│  t = t + Δt       │
└──────────────────┘
         │
         ▼
┌──────────────────┐
│ OUTPUT FILE PROCESSOR│
└──────────────────┘
         │
         ▼
┌──────────────────┐
│ PLOT DEFORMED    │
│ STRUCTURAL GEOMETRY│
└──────────────────┘
```

CALCULATE EIGENVECTORS ← REAL EIGENVALUE EXTRACTION

RECOVER CURRENT DISPLACEMENTS (δ) → FORM STRESS STIFFNESS MATRIX, $K_\sigma = K_\sigma(\delta)$ → PARTITION $[K_\sigma]$

FIGURE 1. - DYNAMIC BUCKLING ANALYSIS SOLUTION SEQUENCE.

```
        ALTER 146      $$$$$ COSMIC NASTRAN RF 09     RELEASE 1987   $$$$$
        PARAML  UPV//*TRAILER*/1/V,N,NOCUPV $$$$$$$$$$$$$$$$$$$$$$$$$$$$$$$$$$$$$
        COPY    TIP1 / CLUSI/ 0 $                                             $
        COPY    TIP1 / BUBLI/ 0 $                                             $
05 PARAM    //*SUB*/SHIFT/NOCUPV/ 1 $                                         $
        LABEL   BUBTOP $<<<<<<<<<<<<<<<<<<<<<<<<<<<<<<<<<<$  BUTLER/PAMIDI     $
        FILE    BUBLI=SAVE/ CLUSI=SAVE $                  $                    $
        PARTN   BUBLI,,BAS1/DUMMY,,,/7 $                  $     BUBBLE         $
        MERGE   DUMMY,,,,,/TIP1/BUBLJ/7 $                 $                    $
10 ADD      CLUSI,BUBLJ/CLUSJ/ $                          $   ALGORITHM        $
        SWITCH  BUBLJ,BUBLI//-1 $                         $                    $
        SWITCH  CLUSJ,CLUSI//-1 $                         $                    $
        REPT    BUBTOP,SHIFT $>>>>>>>>>>>>>>>>>>>>>>>>>>>$                     $
        PARTN   TIP1,,CLUSJ/,MNTRI,,/7 $                                       $
15 PARTN    BUBLJ,,CLUSJ/,BOOTI,,/7 $                                         $
        COPY    MNTRI/MNTRJ/ 0 $$$$$$$$$$$$$$$$$$$$$$$$$$$$$$$$$$$$$$$$$$$$$$$$$$$$$
        TA1     ECT,EPT,BGPDT,SIL,GPTT,CSTM,/X1,X2,X3,ECPT,GPCT,,,,/LUSET/
20              NOSIMP/0/NOGENL/GENEL $
        DPD     DYNAMICS,GPL,SIL,USET/GPLD,SILD,USETD,,,,,,,EED,EQDYN/V,N,
                LUSET/V,N,LUSETD/V,N,NOTFL/V,N,NODLT/V,N,NOPSDL/V,N,NOFRL/
                V,N,NONLFT/V,N,NOTRL/S,N,NOEED/C,N,123/V,N,NOUE $
        COND    ERROR5,NOEED $
        PARAM   //*NOP*/V,N,COLNUM=1 $
        LABEL   RAALOOP $<<<<<<<<<<<<<<    TOP OF RAALOOP     <<<<<<<<<<<<<<<<<$
25 PARAM    //*ADD*/COLNUM/COLNUM/3 $                                         $
        PARAM   //*LE*/V,N,GETOUT/NOCUPV/COLNUM $                             $
        COND    QUITRAA,GETOUT $                                              $
        LABEL   CORTOP $<<<<<<<<<<<<<<<<<<<<<<<<<<<<<<<<<<<<<<<<<<<<<<<<<<<$   $
        PARTN   MNTRJ,,BOOTI/DUM11,,,,/7 $       MOVE THE COLUMN MARKER   $    $
30 MERGE    DUM11,,,,,MNTRI/MNTRJ/7 $        THREE PLACES               $    $
        REPT    CORTOP, 2  $>>>>>>>>>>>>>>>>>>>>>>>>>>>>>>>>>>>>>>>>>>>>>$     $
        PARTN   UPV,MNTRJ,/,,COLUPV,/1 $                                      $
        DSMG1   CASECC,GPTT,SIL,EDT,COLUPV,CSTM,MPT,ECPT,GPCT,DIT/
                KDGG/DSCOSET $                                                $
35 EQUIV    KDGG,KDNN/MPCF2 $                                                 $
        COND    LBL2D,MPCF2 $                                                 $
        MCE2    USET,GM,KDGG,,,/KDNN,,, $                                     $
        LABEL   LBL2D $                                                       $
        EQUIV   KDNN,KDFF/SINGLE $                                            $
40 COND     LBL3D,SINGLE $                                                    $
        SCE1    USET,KDNN,,,/KDFF,KDFS,,,, $                                  $
        LABEL   LBL3D $                                                       $
        EQUIV   KDFF,KDAA/OMIT $                                              $
        COND    LBL5D,OMIT $                                                  $
45 SMP2     USET,GO,KDFF/KDAA $                                               $
        LABEL   LBL5D $                                                       $
        ADD     KDAA,/KDAAM/C,N,(-1.0,0.0)/C,N,(0.0,0.0) $                    $
        READ    KAA,KDAAM,,,EED,USET,CASECC/LAMA,PHIA,MI,OEIGS/C,N,BUCKLING/
                S,N,NEIGV/C,N,2 $·                                            $
50 COND     ERROR4,NEIGV $                                                    $
        PARAML  LAMA//*DTI*/2/3/V,N,EIGV $                                    $
        PRTPARM //0/*EIGV*  $                                                 $
        $OFP    OEIGS,LAMA,,,,//S,N,CARDNO $                                  $
        $OFP    LAMA,,,,,//S,N,CARDNO $                                       $
55 SDR1     USET,,PHIA,,,GO,GM,,KFS,,/PHIG,,BQG/C,N,1/C,N,BKL1 $              $
        SDR2    CASECC,CSTM,MPT,DIT,EQEXIN,SIL,,,BGPDT,LAMA,BQG,PHIG,EST,,/,
                OBQG1,OPHIG,OBES1,OBEF1,PPHIG/C,N,BKL1 $                      $
        $OFP    OPHIG,OBQG1,OBEF1,OBES1,,//S,N,CARDNO $                       $
        COND    P3,JUMPPLOT $                                                 $
60 PLOT  PLTPAR,GPSETS,ELSETS,CASECC,BGPDT,EQEXIN,SIL,,PPHIG ,GPECT,OBES1/
                PLOTX3/V,N,NSIL/V,N,LUSET/V,N,JUMPPLOT/V,N,PLTFLG/S,N,PFILE   $
        PRTMSG  PLOTX3 // $                                                   $
        LABEL   P3 $
        REPT    RAALOOP,1000 $>>>>>>>    BOTTOM OF RAALOOP   >>>>>>>>>>>>>>>>$
65 JUMP     QUITRAA $
        LABEL   ERROR5 $
        PRTPARM //C,N,-3/C,N,BUCKLING $
        JUMP    QUITRAA $
        LABEL   ERROR4 $
70 PRTPARM  //C,N,-4/C,N,BUCKLING $
        LABEL   QUITRAA $
        JUMP    FINIS $
        ENDALTER


     BULK DATA
     DMI    TIP1    0    2        1        1          1000    1
     DMI    TIP1    1    1        1.0
     DMI    BAS1    0    2        1        1          1000    1
     DMI    BAS1    1    1000     1.0
```

FIGURE 2. - DYNAMIC BUCKLING DMAP ALTER FOR TRANSIENT SOLUTION SEQUENCE.

1.0 IN. DIAM

P(t) →

|← 100 IN. LENGTH →|

(A) GEOMETRY.

$$P_{cr} = \frac{\pi^2 EI}{4L^2}$$

P(t)

25 μs

TIME

(B) LOADING.

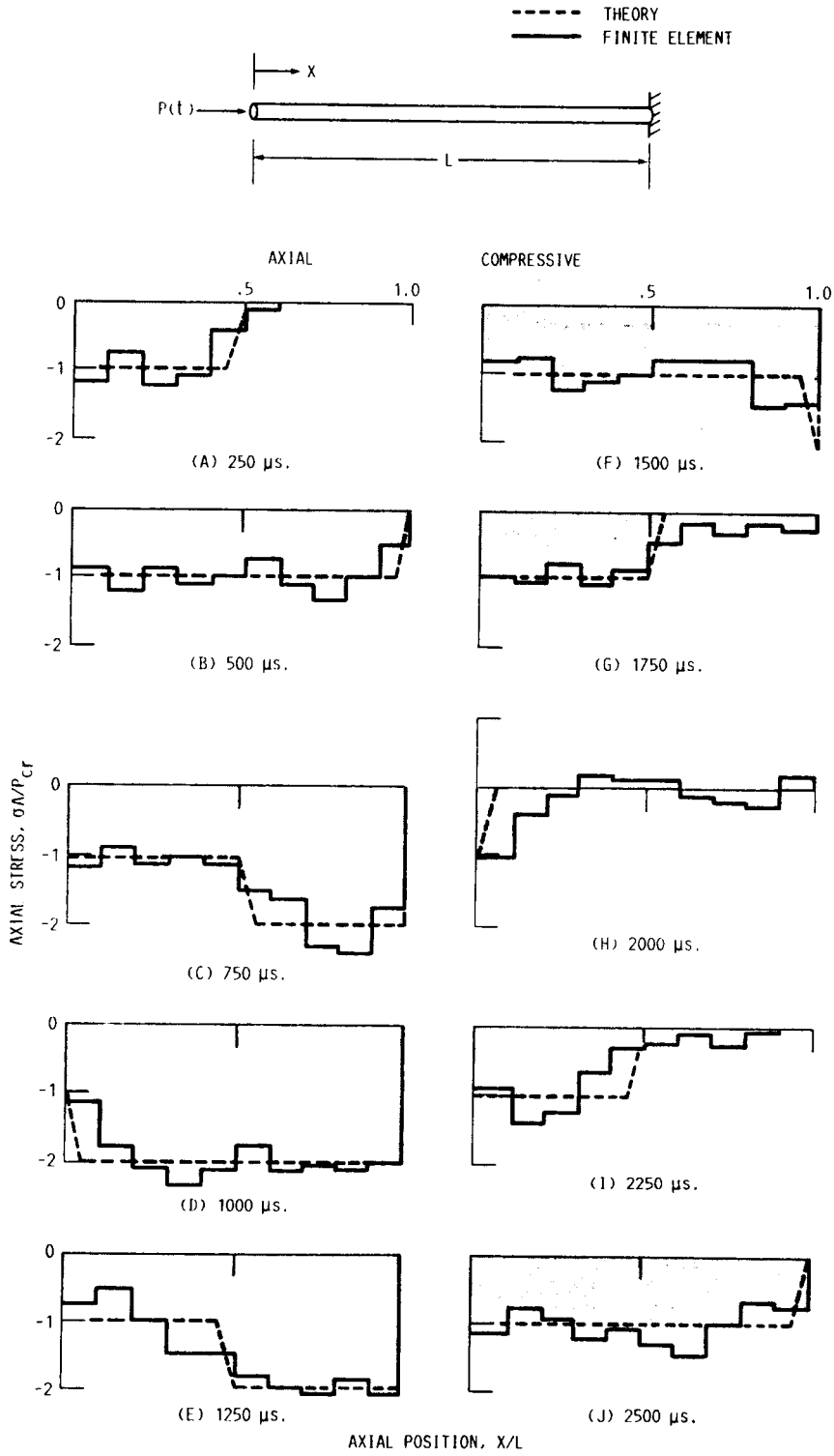FIGURE 3. - EXAMPLE PROBLEM GEOMETRY AND LOADING: LONGITUDINAL IMPACT OF A UNIFORM BAR.

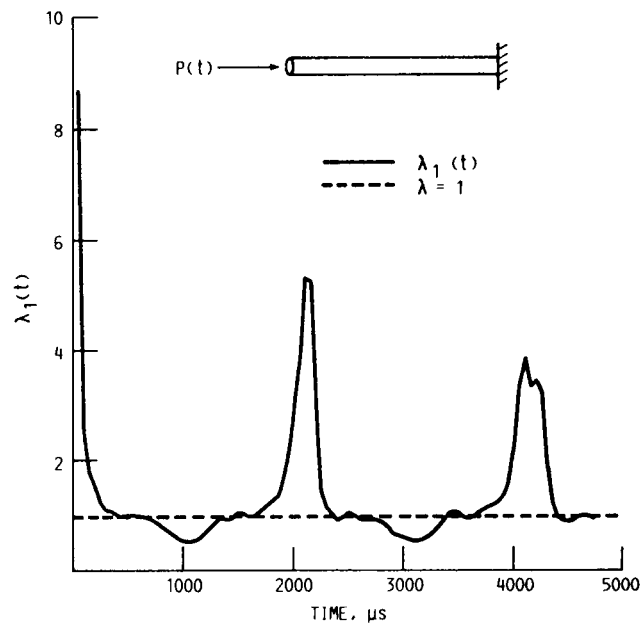FIGURE 4. - AXIAL STRESS DISTRIBUTION IN BAR DUE TO LONGITUDINAL IMPACT.

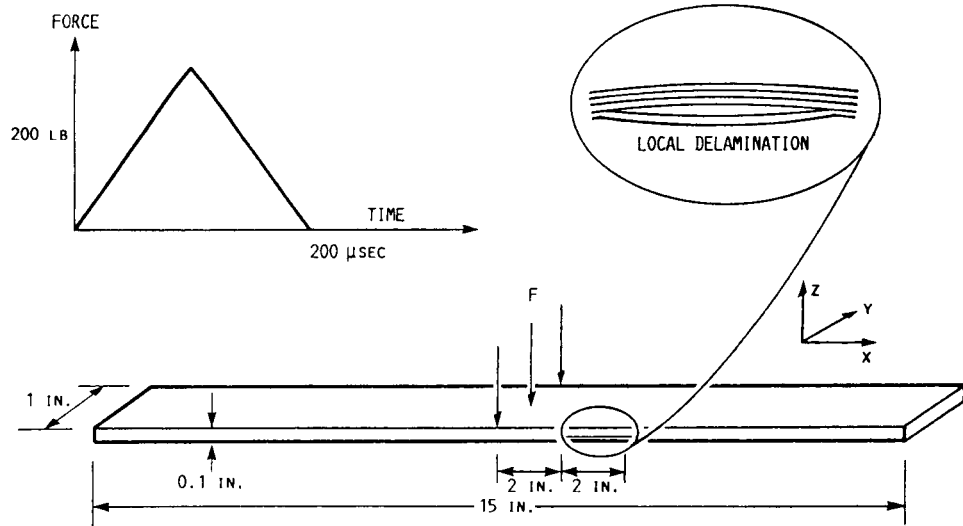FIGURE 5. - TIME DEPENDENCE OF FIRST EIGENVALUE IN
EXAMPLE PROBLEM.

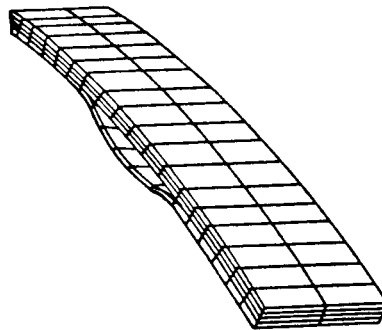FIGURE 6. - COMPOSITE LAMINATE WITH INITIAL DELAMINATION.

FIGURE 7. - FINITE ELEMENT REPRESENTATION
OF COMPOSITE LAMINATE SHOWING LOCAL BUCK-
LING OF THE DELAMINATED PLIES.
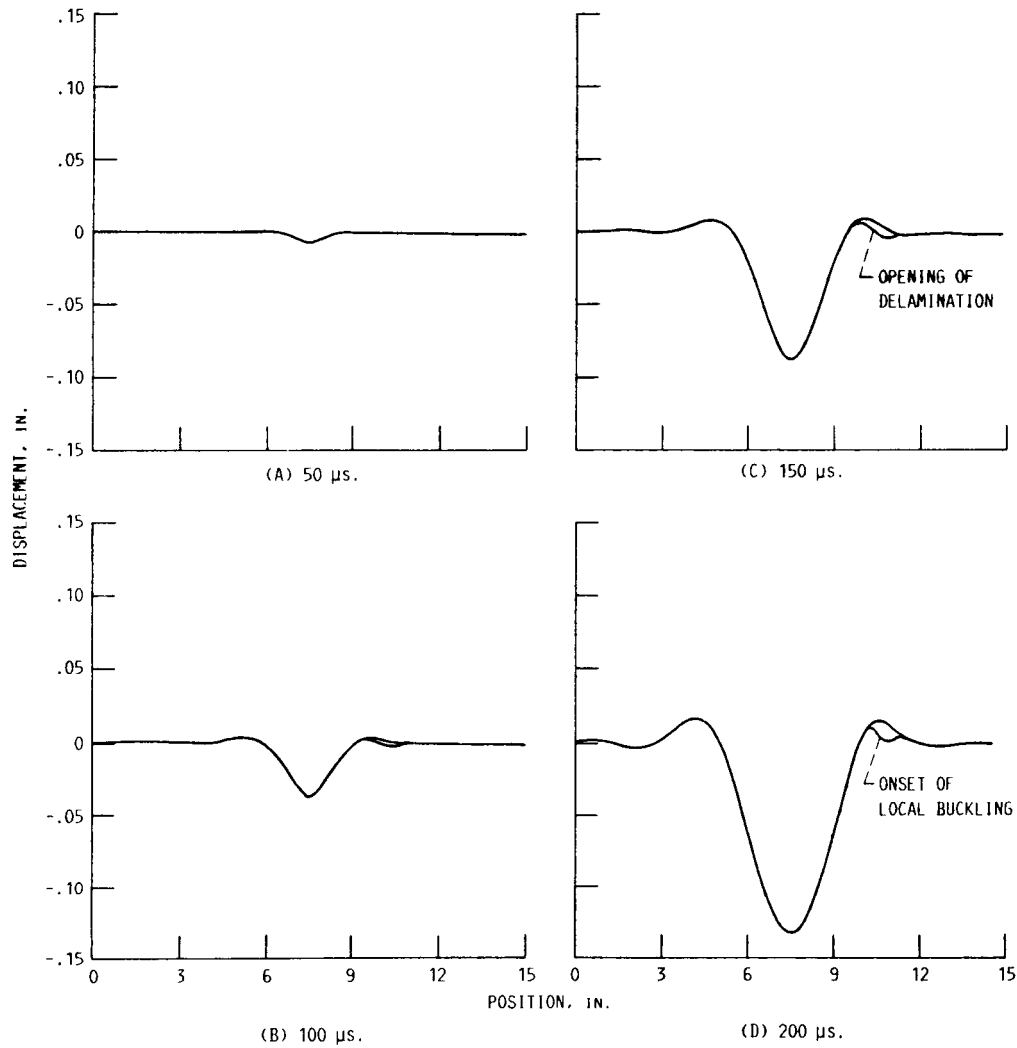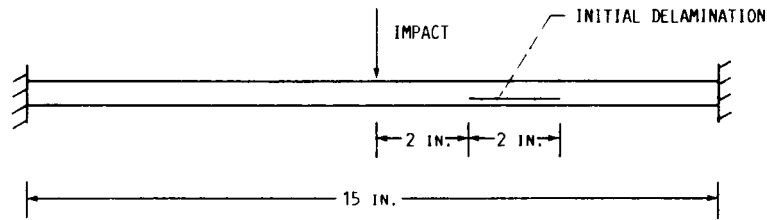
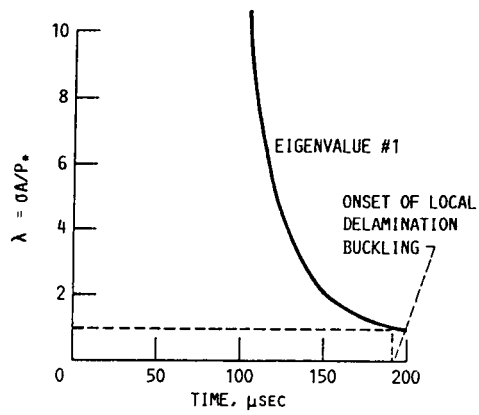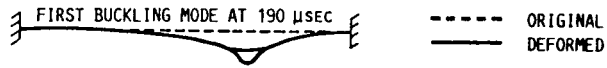FIGURE 8. - MIDPLANE DISPLACEMENT PROFILES OF IMPACTED LAMINATE.

199

FIGURE 9. - TIME DEPENDENCE OF LOWEST EIGENVALUE FOR COM-
POSITE LAMINATE SUBJECTED TO TRANSVERSE IMPACT.